Journal of Electroanalytical Chemistry 907 (2022) 116030

Contents lists available at ScienceDirect

Journal of Electroanalytical Chemistry

journal homepage: www.elsevier.com/locate/jelechem

Computational design and fabrication of a highly selective and sensitive molecularly imprinted electrochemical sensor for the detection of enzalutamide

S.Irem Kaya [a,b], Ahmet Cetinkaya [a], Goksu Ozcelikay [a], M. Emin Çorman [a,c,*], Mustafa Karakaya [d], Esen Bellur Atici [e], Sibel A. Ozkan [a,*]

[a] Ankara University, Faculty of Pharmacy, Department of Analytical Chemistry, Ankara, Turkey
[b] University of Health Sciences, Gulhane Faculty of Pharmacy, Department of Analytical Chemistry, Ankara, Turkey
[c] University of Health Sciences, Gulhane Faculty of Pharmacy, Department of Biochemistry, Ankara, Turkey
[d] Sinop University, Faculty of Engineering & Architecture, Department of Energy System, Sinop, Turkey
[e] DEVA Holding A.S. R&D Center, Tekirdag, Turkey

ARTICLE INFO

Keywords:
Enzalutamide
Molecularly imprinted polymer
Aniline
O-phenylenediamine
Electrochemical determination
Voltammetry
Drug analysis

ABSTRACT

This study demonstrates the first electrochemical analysis of an anti-androgen drug enzalutamide with a molecularly imprinted polymer (MIP)-based sensor. An electrochemical sensor was developed through computational approaches for screening functional monomers in the rational design of MIPs. Based on the computational approach, ortho-phenylenediamine (o-PD) was selected as a functional monomer based on the comparison of interaction energies (ΔE) between enzalutamide and monomers. The characterization of the MIP-based sensor was investigated by Raman spectroscopy, surface electron microscopy (SEM), contact angle measurements, and electrochemical techniques. Different electrochemical techniques such as differential pulse voltammetry (DPV) and electrochemical impedance spectroscopy (EIS) were utilized for the evaluation of MIP parameters (removal process, incubation time, monomer ratio etc.). MIP@ANI-*co*-o-PD/GCE showed a linear response in the concentration range between 1×10^{-16} M and 1×10^{-15} M with the limit of detection (LOD) and limit of quantification (LOQ) values of 0.019 fM and 0.065 fM, respectively. The application studies from human serum and pharmaceutical dosage form samples were concluded with good recovery results demonstrating the sensor's applicability, selectivity, precision, and accuracy. Furthermore, selectivity studies were carried out with similarly structured compounds teriflunomide and leflunomide. Lastly, the non-imprinted polymer (NIP) based electrochemical sensor was prepared and used for the performance evaluation of the MIP@ANI-*co*-o-PD/GCE sensor.

1. Introduction

Enzalutamide (ENZA) [4-(3-(4-cyano-3-(trifluoromethyl)phenyl)-5,5-dimethyl-4-oxo-2-thioxoimidazolidin-1-yl)-2-fluoro-*N*-methylbenzamide] is a novel androgen receptor inhibitor that is the most frequently used drug for treatment of patients with metastatic castration-resistant prostate cancer (mCRPC) [1]. ENZA therapy is mostly initiated in male patients who do not respond well to hormone therapy. It is recommended to be taken before or after chemotherapy. ENZA aims to reduce prostate cancer cell proliferation and reduce prostate-specific antigen (PSA) levels in the serum. ENZA is found as 40 mg of capsule form. It should be taken orally at a dosage of 160 mg/per day [2]. ENZA can cause common/less common side effects such as extreme tiredness, feeling nervous, severe headaches, swelling of the breast area, dry or itchy skin, high blood pressure, and problems with memory and concentration [3]. ENZA contains benzamides, an imidazolidinone, a nitrile, (trifluoromethyl)benzenes, and monofluorobenzenes.

The most used analytical techniques for the determination of ENZA in biological samples and/or pharmaceutical dosage forms are liquid chromatography with UV–vis [4–11] and MS detection [12,13]. Nevertheless, these techniques suffer from drawbacks such as high-cost equipment, tedious procedures, and labor-intensive. Therefore, an effective method for fast and real-time analysis of drugs is still a crit-

* Corresponding author at: Ankara University, Faculty of Pharmacy, Department of Analytical Chemistry, Ankara, Turkey
E-mail addresses: mehmetemincorman@gmail.com (M.E. Çorman), ozkan@pharmacy.ankara.edu.tr (S.A. Ozkan).

https://doi.org/10.1016/j.jelechem.2022.116030
Received 19 November 2021; Received in revised form 1 January 2022; Accepted 6 January 2022
Available online 10 January 2022

ical challenge in practical applications. Due to the ease of use (simplicity), fast response, and affordable assay, electrochemical sensors offer several advantages over other methods [14]. Furthermore, it gives many opportunities due to the point of care devices in pharmaceuticals, clinical, and environmental analyses [15]. Compared to the other working electrodes, different types of carbon-based electrodes are generally preferred due to their strong mechanical properties, chemical resistance, reusability, and stability [16]. However, electrochemical sensors may have some challenges, such as low sensitivity and selectivity, and stability. The molecularly imprinting technique has emerged as a promising synthetic material for improving the requirements of electrochemical sensors. Molecular imprinting is well known as synthetic biomaterials or artificial receptor that results in selective cavities in a 3D-polymeric network [17]. MIPs involve three main steps: pre-polymerization complexes formation between monomer and template; functional monomer polymerization around the template molecule and template removal that resulted in creating recognition sites which are complementary to the template in size, shape and functional group orientation [18,19] MIPs based electrochemical sensors offer significant advantage as compared to biological-based sensors using enzymes or antibodies [20,21]. Furthermore, molecularly imprinted electrochemical sensors (MIECS) showed excellent recognition properties in the sensor field compared to other detection methods due to higher selectivity, sensitivity, and lower cost [22]. The most suitable monomer and the optimal molar ratio of the template also are required for the logic synthesis of MIPs with imprinting efficiency. Therefore, computational approaches play important roles in understanding and imagining the molecule configurations that provide effective molecular modeling of MIP. Computational methods rely on theoretical calculations and the accuracy of the measured interaction energies of the molecular system. Furthermore, computational approaches avoid using disposable chemicals and provide advantages such as low costs, time savings, clinical and environmental safety. [23,24].

In this study, MIP for ENZA was firstly computationally designed, and electrochemical sensors were developed on the glassy carbon electrode by electropolymerization for the selective and sensitive determination of ENZA in pharmaceutical dosage form and synthetic human serum samples. While aniline (ANI) is identified as one of the best-conducting monomers, o-phenylenediamine has emerged as an alternative monomer for improving sensors' active site and performance due to its ease of copolymerization with ANI and free amino group subsequent to conjugation [25]. Therefore, copolymerization of the ANI-*co*-o-PD couple was investigated to determine the optimal ratio of monomer and template in designing and synthesizing the MIPs. MIP-based electrochemical sensors were developed and then characterized by spectroscopic and electrochemical techniques based on the computational design. The MIP parameters were evaluated to get the best electrochemical sensors of ENZA in a different medium. Then, the developed electrochemical MIP sensors were selectively applied to the pharmaceutical dosage form and synthetic human serum samples. MIP and NIP signals were evaluated, and imprinting factors (IF) were discussed. Then, the selectivity of the sensor that is a critical parameter for MIP sensors was performed using similar competitive drugs, leflunomide and teriflunomide. The precision, accuracy, selectivity, and sensitivity parameters were also evaluated. By this approach, the developed MIECS offered an attractive alternative for a fast, cost-effective, fully validated selective electrochemical MIP sensor for the sensitive determination of ENZA.

2. Experimental

2.1. Reagents and chemicals

ENZA active ingredient and tablet dosage form were provided by DEVA Holding A.Ş (Istanbul, Turkey). Drug-free human serum, acetic acid (≥99%), sodium hydroxide (>97%), sodium acetate trihydrate (>99%), methanol (99.8%), and o-PD (≥98%) were supplied from Sigma-Aldrich. Potassium ferricyanide (99%), and potassium ferrocyanide (99%), were obtained from Merck.

All of the materials used during the experiment were not pre-treated and were used directly. 1.0 mM ENZA drug stock solution was prepared in pure methanol and sonicated for 10 min. Standard solutions were prepared by taking a certain amount of the stock solution and using the supporting electrode. All electrochemical measurements were prepared using double distilled water and stored in the refrigerator at 4 °C.

2.2. Instruments

Electrochemical measurements such as CV and DPV were performed using an AUTOLAB (Netherlands) controlled by NOVA 2.1.4 software. EIS studies were also carried out using the same device extended with the EIS module (Metrohm). Electrochemical experiments were carried out using the conventional three-electrode system with GCE (3.0 mm diameter) as the working electrode, Ag/AgCl electrode (3 M KCl) as the reference electrode, and platinum wire as the counter electrode. The chemicals used in the experimental studies were weighed using precision balances (Ohaus Instruments, Shanghai-China). The pH of the supporting electrolyte solution was checked with a pH meter (Mettler-Toledo pH/ion S220, Switzerland). Removal and rebinding processes were performed by Thermo-Shaker (Biosan TS-100)

2.3. Preparation of the MIP and NIP based electrochemical sensors

GCE was sonicated in a solution containing methanol and double distilled water (1:1, v/v) for 15 min before experimental studies. After that, the electrode surface was cleaned using alumina slurry on the polishing pad, washed with double-distilled water, and dried at room temperature.

Bare GCE was pre-treated in a pH 5.2 acetate buffer solution for 15 cycles using CV in the potential range of −0.2 V to 1.2 V. Electropolymerization (EP) was achieved as follows: monomer solution was prepared by dissolving a supporting electrolyte medium containing ANI, and pre-polymerization o-PD-ENZA complex (molar ratio 3:1) and then polymerization was performed using CV technique with 5 cycles at a potential range of −0.2 V to 1.2 V, scan rate of 50 mV/s (Fig. 1.

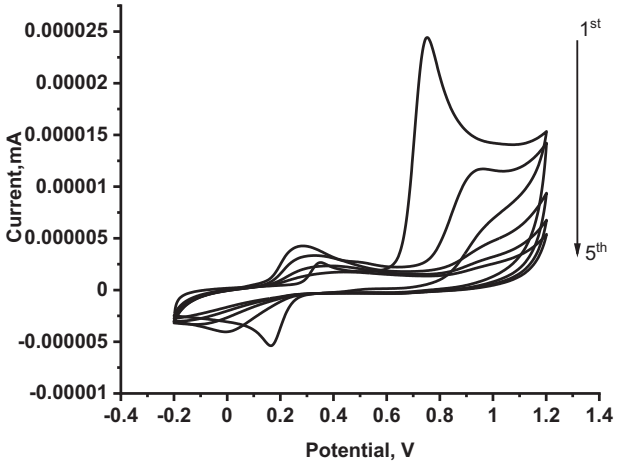

Fig. 1. Cyclic voltammograms of the EP process in the mixture of 0.02 mM ENZA, 0.80 mM ANI, and 0.05 mM o-PD solution with 5 cycles at a scan rate of 50 mV/s.

After EP, the GCE surface was rinsed with double-distilled water and then template molecule ENZA was removed by acetic acid solution for 20 min using Thermo-Shaker (650 rpm, 25 °C). Subsequently, the rebinding process in different concentrations of ENZA was performed under the same optimization conditions of the MIP-based electrode and using the same shaker device for 5 min. Before each incubation, the electrode was washed with distilled water for 50 s. Finally, non-imprinted polymer (NIP) based electrode was also prepared using the same procedure in the absence of template molecule ENZA for comparison purposes.

Using different techniques such as CV, DPV, and EIS, all electrochemical measurements of MIP and NIP-based sensors were performed in a solution prepared in 100 mM KCl containing 5 mM $[Fe(CN)_6]^{3-/4-}$.

2.4. Computational details

The counterpoise (CP) approach was applied in corrected/uncorrected energies, basis set superposition error (BSSE) energies and complexation energies. All the interaction simulations, CP calculations, geometric optimizations, and parameters were accomplished in restricted Hartree-Fock (RHF) theory [26,27], which is one of the basic approximate methods to solve the many-body Hamiltonian with 6-31G (d) basis set [28,29]. Gauss View software was used for selecting interaction components (ENZA with ANI and *o*-PD) as Gaussian fragments X and Y and the description of atomic coordinates [30]. Total self-consistent field (SCF) energies, CP energies, hydrogen bond geometries, and essential torsion angles between the interactions were computed by the Gaussian 09 W program [31] in all the optimization processes [32].

2.5. Characterization of the molecularly imprinted electrochemical sensor surface

The surface morphology of the MIECS was examined by using scanning electron microscopy (SEM, TESCAN GAIA 3, Brno – Kohoutovice, Czech Republic). To confirm the characteristic functional groups of ANI-*co*-o-PD, a Raman spectrometer was used with an operation range of 200–200 cm^{-1} at a 785 nm laser source (JASCO NRS-4500 Confocal Raman Microscope). The contact angle of the electrochemical electrodes was determined with the KRUSS DSA100 (Hamburg, Germany) instrument. With the Sessile Drop method, the contact angle of the chip surface was measured by dropping one drop. Contact angle values were obtained from the left contact point of the droplet with solid.

2.6. Pharmaceutical dosage form and real sample application

For the assay and the recovery studies from the tablets, the average weight of five tablets containing approximately 40.0 mg of ENZA was weighed and homogenized by pulverizing in a mortar. 1.0 mM drug stock solution prepared using pure methanol was sonicated for approximately 15 min, and then the mixture was filtered. The measurement solution was prepared by taking the required amount of the filtered solution and using the supporting electrolyte solution (pH 5.2 acetate buffer). Previously obtained calibration data were used to determine the amount of ENZA in pharmaceutical samples.

The recovery study was carried out to verify the accuracy of the DPV method after adding a controlled aliquot of ENZA at standard concentrations to the tablet dosage form.

Serum samples were removed from the –20 °C in the freezer and thawed at room temperature. In order to prepare the 0.1 mM standard serum solution, a 3.6 mL aliquot of serum was transferred to 1.0 mL of drug solution into the test tube, and 5.4 mL of acetonitrile was added to induce the precipitation of proteins. Tubes were sonicated for 15 min, then centrifuged (5000 rpm, 20 min) to precipitate protein residues. A calibration plot of the supernatant prepared in pH 5.2 acetate buffer was obtained in a certain concentration range. The recovery study was performed by taking five different measurements at the best reproducible concentration and adding a standard sample of the drug at known concentrations.

3. Results and discussion

3.1. Quantum calculations for designing of MIP

In the first stage of our work by computational methods, we aim to compare the interactions of the target molecule with ANI and o-PD monomers. In this study performed in HF method and the lower-level basis set (3-21G), the corrected ΔE values are −19.87 and −35.69 kJ/mol for the ANI and o-PD monomers, respectively. It is considered that the o-PD interaction is more effective than ANI.

In Fig. 2, optimizations show the ENZA structure and its interactions with monomers in the HF method. N—H···N_4, N—H···O1, and N—H···O_2 hydrogen bonds are seen in the o-PD ([A])-ENZA ([B]) interactions (Fig. 2. b, c, and d). In addition, the total energies of all o-PD-ENZA interactions and the uncorrected (raw) and corrected interaction energies (ΔE) obtained by CP approach are given in Table 1. The difference between the corrected and uncorrected interaction energy gives the BSSE energy correction. In our study, each of the optimizations [A]…[B] and 2[A]…[B] has three different interaction geometries according to the total SCF energy values calculated by HF/6-31G(d) approach. ΔE (corrected) values for each [A]…[B] forms are −26.53, –23.35 and −17.41 kJ/mol. For 2[A]…[B] optimal structures, they are −50.87, −43.35 and −40.67 kJ/mol. The strongest interactions with the minimum total SCF value in different forms of [A]…[B] and 2[A]…[B] are reported in Table 1 as the most stable structures. The uncorrected and corrected ΔE in 3[A]…[B] structure is calculated as −89.20 and −65.16 kJ/mol, respectively. The order of the uncorrected and corrected ΔE values is 3[A]…[B] > 2[A]…[B] > [A]…[B]. In summary, the interactions of the ENZA molecule are strongest in 3[A]…[B] modeling and weakest in [A]…[B] modeling.

Table 2 shows the hydrogen bond geometries and the all-interaction geometries in [A]…[B], 2[A]…[B] and 3[A]…[B] optimizations. Deformations on essential torsion angles for ENZA structure are also recorded in Table 2. [A]…[B] interaction affects C3-N2-C4-C5 and C6-C7-C8-N3 dihedral angles with a distance of 2.022 Å (N—H···O1). In 2[A]…[B] interaction, H···N4 and H···O1 distances result as 2.429, and 2.119 Å, respectively, and all essential torsion angles are markedly deformed. Table 2 shows that the most effective deformation is in the 3[A]…[B] interaction geometries. The N—H bond lengths on the monomers range 0.999–1,002 Å in all interaction models.

3.2. Surface characterization of MIECS.

The surface morphology of MIECS under optimized conditions was examined using SEM (Fig. 3A. The SEM images clearly show that the surface roughness of the sensor is stemmed from the formation of polymer nanofilm by EP of the ANI-*co*-o-PD onto the surface of the electrode. Fig. 3B shows the several characteristic bands originating from ANI-*co*-o-PD polymeric surface. The characteristic Raman bands of ANI-*co*-o-PD were observed at 1168 cm^{-1} for (C—H) stretching, 1293 cm^{-1} (C-NH_2) stretching 1383 cm^{-1} (C—N +) stretching ring deformation, 1493 cm^{-1} for in-plane bending (C=C) in phenyl ring, and 1593 cm^{-1} for (C=C) stretching of the phenyl ring. From the above results, it was confirmed that polymerization was successfully achieved on the GCE surface. In addition, contact angles were calculated for further characterization of MIECS (Fig. 3C and D. The bare GCE electrode surface was 80.1°. After EP of MIP film on the GCE, the contact angle of the sensor surface was decreased to 57.2° due to the introduction of the hydrophilic characters of monomers onto the

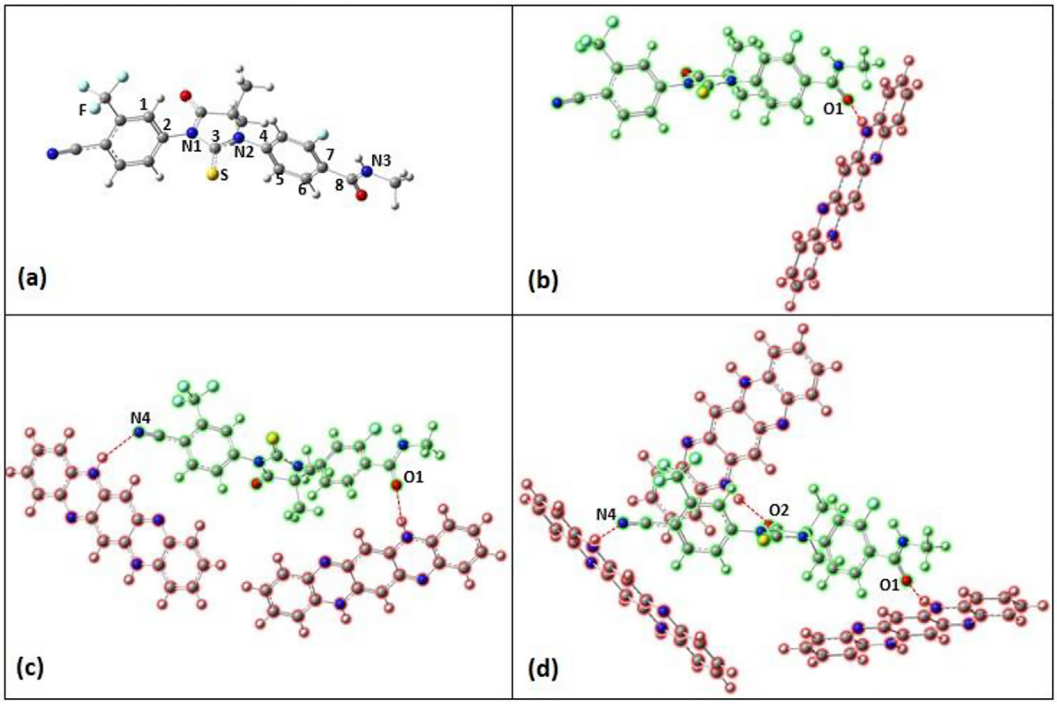

Fig. 2. The optimizations of **(a)** ENZA and *o*-PD-enza interactions, **(b)** [A]…[B], **(c)** 2[A]…[B], **(d)** 3[A]…[B]

Table 1
Total energies and uncorrected/corrected interaction energies (ΔE) in monomers-ENZA interactions by the computational method.

Structures	Total SCF Energy (a. u)	Uncorrected ΔE (kJ/mol)	Corrected ΔE (kJ/mol)
[B]	−1967.4015		
[A]…[B]	−2873.8363	−32.84	−26.53
2[A]…[B]	−3780.2711	−65.17	−50.87
3[A]…[B]	−4686.7045	−89.20	−65.16

surface. These results indicate that the MIP film was successfully formed on the GCE surface.

3.3. Electrochemical characterization of MIP@ANI-co-o-PD/GCE

CV and EIS measurements using 5 mM $[Fe(CN)_6]^{3-/4-}$ solution as the redox probe were performed for the electrochemical characterization of MIP@ANI-*co*-o-PD/GCE. Fig. 4a, shows the CV voltammograms of the GCE at the various steps of the sensor preparation. As shown in Fig. 4a, the highest oxidation peak belongs to the bare GCE, followed by after removal, after incubation of ENZA, and after EP, respectively. Fig. 4b shows the Nyquist plots of the same steps of the sensor preparation as above, obtained by EIS. The results demonstrated that the highest charge transfer resistance (R_{ct}) value was acquired for the GCE after EP (31339 Ω), followed by after rebinding of ENZA (321.59 Ω), after removal (208.96 Ω), and for bare GCE (141.39 Ω). Those results can be explained by the obstructed electron transfer after the polymer formation on the electrode surface. While the removal process forms the cavities and increases the electron transfer, rebinding of ENZA significantly decreases the signal of $[Fe(CN)_6]^{3-/4-}$.

3.4. Optimization of experimental conditions

3.4.1. Ratio of ANI to o-PD and template

For the formation of an effective and stable MIP, selecting the most suitable monomers and determining the molar ratios are the most critical factors. In the beginning, ANI and o-PD were examined individually. When ANI was used alone, the results showed that the polymer was not stable enough and was decomposed after the removal process. On the other hand, polymerization using only o-PD resulted in a low-efficiency removal. Therefore, ANI and o-PD were used to form a more efficient, more stable, and selective copolymer. The ratio of ANI to *o*-PD was decided by studying different ratios of ANI:*o*-PD-ENZA (20:3:1, 30:3:1, 40:3:1, 50:3:1, 60:3:1) while keeping the template ratio constant at 1 and the o-PD ratio at 3. When the difference between peak currents after EP and after removal was compared (Fig. 5a, 40:3:1 with the highest value was chosen as the optimal ratio with better removal and stability properties.

3.4.2. Number of cycles for copolymerization

The number of cycles for copolymerization is a parameter that directly affects the stability and thickness of the polymer film. 3, 5,

Table 2
Hydrogen-bond geometry and essential torsional (dihedral) angle in monomers-ENZA interactions by the computational method.

Structures	d(H···N4) (Å)	d(H···O1) (Å)	d(H···O2) (Å)	C1-C2-N1-C3 (°)	C3-N2-C4-C5 (°)	C6-C7-C8-N3 (°)
[B]	–	–	–	109.52	93.61	−172.76
[A]···[B]	–	2.022	–	109.54	96.17	−159.91
2[A]···[B]	2.429	2.119	–	83.31	85.44	−154.77
3[A]···[B]	2.406	2.117	2.199	78.14	86.73	−155.04

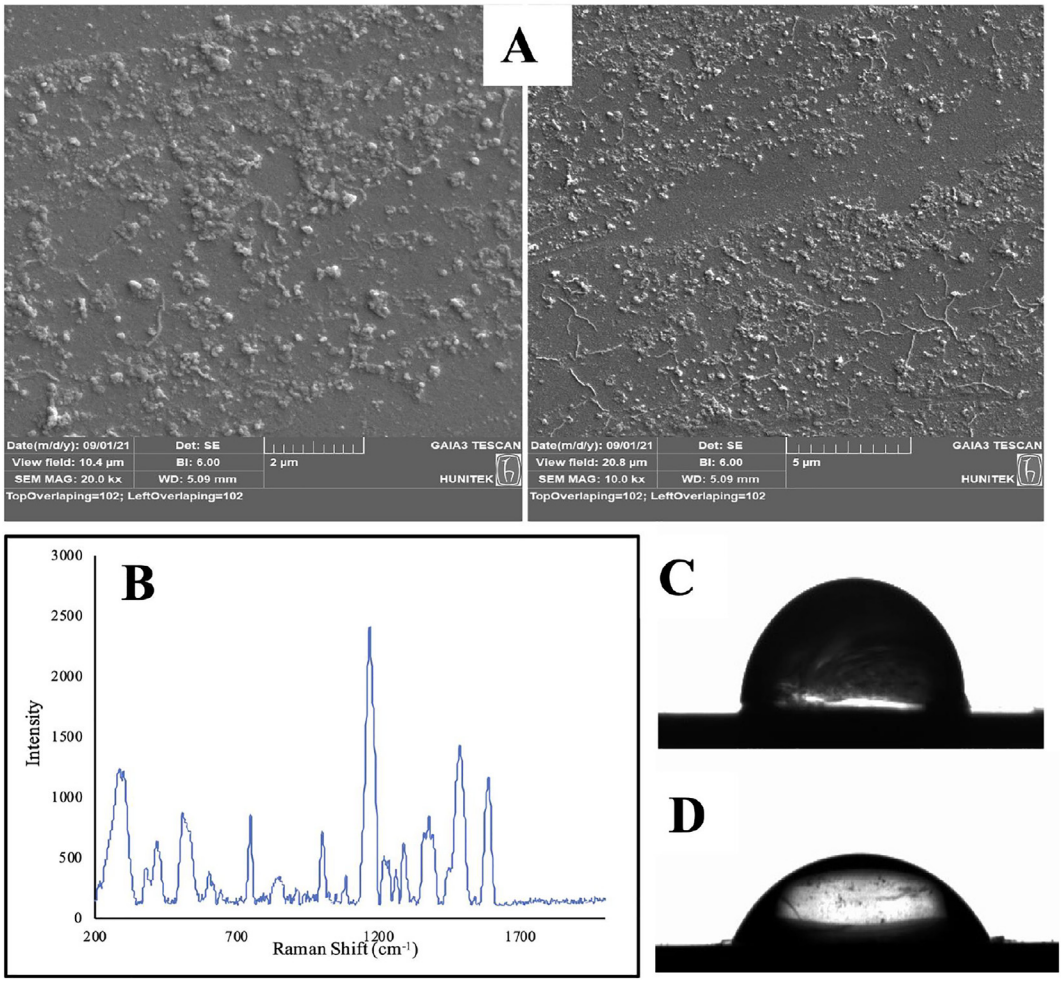

Fig. 3. **(A)** SEM images of MIECS; **(B)** Raman spectra of MIECS; **(C)** Contact angel measurements of bare GCE electrode and **(D)** MIECS.

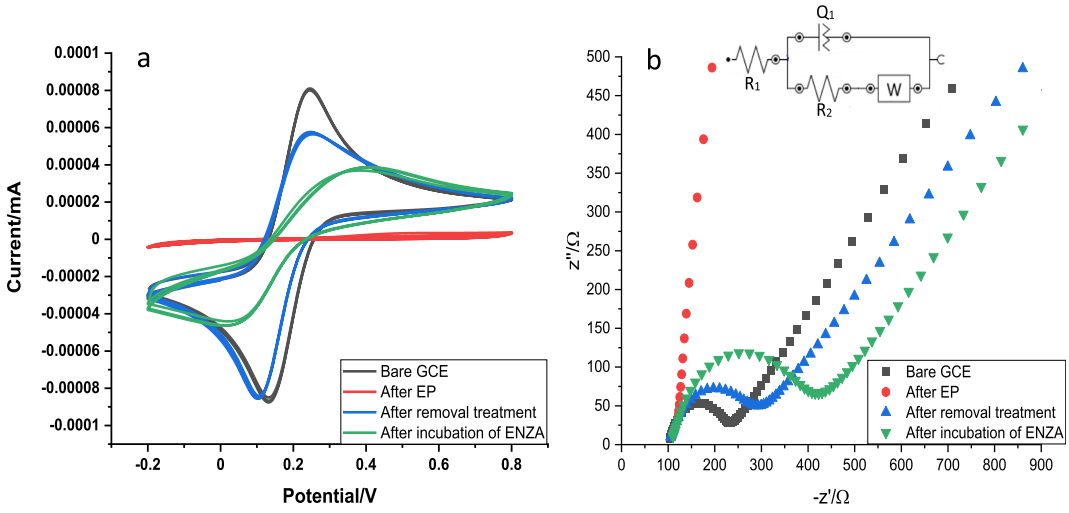

Fig. 4. a) CV, b) EIS measurements of GCE before EP, after EP, after removal treatment and after incubation of ENZA in 5 mM $[Fe(CN)_6]^{3-/4-}$ solution.

7, and 10 cycles were evaluated for the optimization of this parameter. The difference between obtained peak currents after removal and after EP was assessed, and it was seen that this value significantly increases at 5 cycles and sharply decreases after 5 cycles. It can be explained by the difficulty of removal as the thickness of the polymer film increases. Therefore, 5 cycles were chosen for the electrochemical copolymerization of ANI and o-PD.

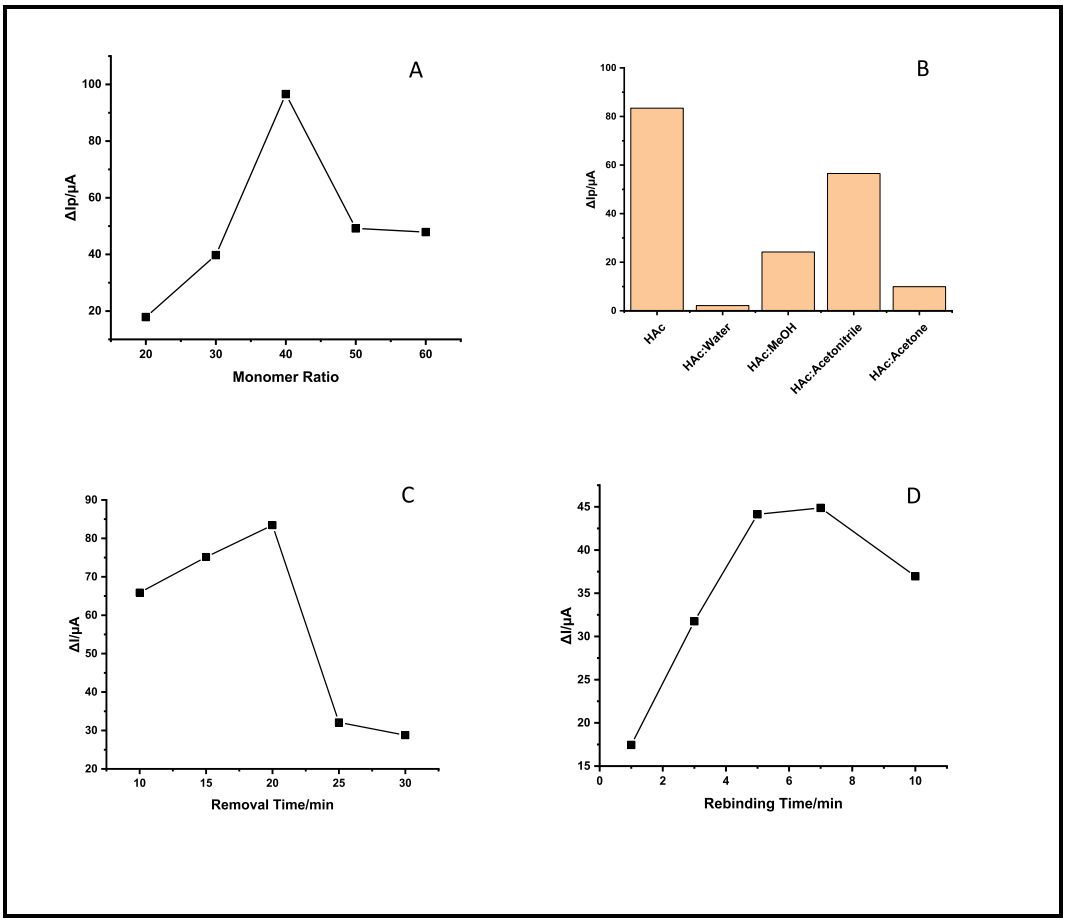

Fig. 5. The plot of ΔIp values versus **(a)** different ANI ratios, **(b)** different removal solutions, **(c)** different removal times, **(d)** different incubation times.

3.4.3. Removal of the template

For the optimization of the template removal process, different removal solutions and times were tested. 15 M acetic acid solution and its 1:1 (v/v) mixtures with double distilled water, methanol, acetonitrile, and acetone were applied for 20 min (Fig. 5b. When the difference between peak currents after removal and after EP was evaluated, it was found that 15 M acetic acid solution has the most efficient removal and stability. Hence, it was tested for removal time optimization. For this purpose, MIP@ANI-*co*-o-PD/GCE was immersed into 15 M acetic acid solution for 10, 15, 20, 25, and 30 min using a Thermo-Shaker at 650 rpm. As it can be seen in Fig. 5c, the best result, followed by a sharp increase, was obtained with 20 min.

3.4.4. Incubation time

The incubation time of ENZA is associated with the sensor response time; therefore, it should be evaluated carefully. 1, 3, 5, 7, and 10 min were studied to optimize the incubation time of 1×10^{-4}M ENZA using a Thermo-Shaker at 650 rpm. The difference between the peak currents after removal and after rebinding of 1×10^{-4}M ENZA (ΔI_p) was calculated for each incubation time. Fig. 5d shows that 5 min and 7 min have almost the same results as the two best options. Consequently, in order to achieve a shorter analysis time, 5 min of incubation time for ENZA was chosen as optimal.

3.5. Analytical performance of MIP@ANI-co-o-PD/GCE

Analytical performance of the MIP@ANI-*co*-*o*-PD/GCE was assessed using various ENZA concentrations in the range between 0.1 fM and 1 fM under the optimized experimental conditions utilizing DPV method and 5 mM $[Fe(CN)_6]^{3-/4-}$ solution (Table 3. MIP@ANI-*co*-o-PD/GCE sensor showed a linear response for selective and sensitive ENZA determination and the regression equation was found as ΔI_p(-μA) = $2.624 \times 10^{16} C$ (M) + 42.458 (R^2 = 0.999). LOD and LOQ values were calculated as 0.019 fM and 0.065 fM using the equations of LOD = 3 s/m and LOQ = 10 s/m. In order to control the analytical performance and evaluate the selectivity, the same concentration range of ENZA was applied to NIP-based sensor. Fig. 6A shows the decreased $[Fe(CN)_6]^{3-/4-}$ peaks versus increased ENZA concentrations. ΔI_p values versus ENZA concentration plots for MIP and NIP-based sensors are given in Fig. 6B.

Table 3
Regression data of the calibration line for ENZA on MIP@ANI-*co*-o-PD/GCE.

	Standard solution	Serum sample
Linearity range (fM)	0.1–1	0.1–1
Slope (μA M^{-1})	2.624×10^{16}	2.127×10^{16}
SE of slope	3.80×10^{14}	5.29×10^{14}
Intercept (μA)	42.458	76.502
SE of intercept	0.233	0.325
Correlation coefficient (*r*)	0.999	0.999
LOD (fM)	0.019	0.029
LOQ (fM)	0.064	0.098
Repeatability of peak current (RSD%)*	0.808	1.212
Reproducibility of peak current (RSD%)*	1.603	2.016

* Each value is the mean of three experiments.

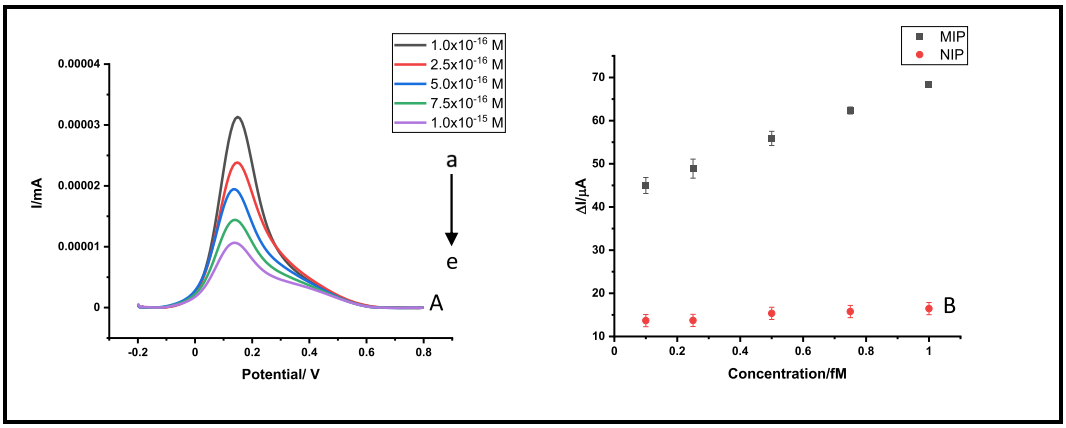

Fig. 6. **(A)** DPV of the MIP@ANI-*co*-o-PD/GCE with increasing ENZA concentration in buffer solution: ENZA concentration was (a) 0.1 fM, (b) 0.25 fM, (c) 0.5 fM, (d) 0.75 fM, (e) 1 fM, respectively. **(B)** The calibration curve of ENZA using MIP@ANI-*co*-o-PD/GCE and NIP@ANI-*co*-o-PD/GCE. The measurement was performed in 5 mM $[Fe(CN)_6]^{3-/4-}$ solution/0.1 M KCl. Scan rate: 100 mV s^{-1}.

3.6. Application in human serum and tablet dosage form

Tablet dosage form and serum samples were chosen for the evaluation of the sensor's applicability. The obtained DPV voltammograms after rebinding of different ENZA concentrations are showed in Fig. 7A. ΔIp values versus ENZA concentration plots for MIP and NIP-based sensors are given in Fig. 7B. The regression data of ENZA determination in serum samples using MIP@ANI-*co*-o-PD/GCE were summarized in Table 4. LOD and LOQ values for the serum sample were found as 0.029 fM and 0.098 fM, respectively. The recovery results related to tablet dosage form and serum sample were found as 101.78% and 98.56%. The results were given in Table 4, confirming that the MIP@ANI-*co*-o-PD/GCE showed satisfactory recovery for ENZA in real samples.

Table 4
Results of the tablet dosage form and recovery experiments.

	Tablet dosage form (XTANDI®)	Serum sample
Label amount (mg)	40.00	–
Found amount (mg)	40.38	–
RSD%*	2.43	–
Bias%	0.95	–
Spiked amount (mg)	4.00	1.00
Found amount (mg)	4.07	0.99
Average recovery (%)	101.78	98.56
RSD% of recovery*	2.10	1.54
Bias%	1.78	−1.44

* Each value is the mean of three experiments.

3.7. Imprinting factor

Imprinting factor (IF) is a key feature of MIP for evaluating the sensor's selectivity. The selectivity studies were performed with structural and chemically similar compounds. For this purpose, leflunomide and teriflunomide were chosen as the competitive drugs. The IF was calculated as the ratio of the ΔI_p values of MIP to NIP-based sensors after the rebinding of 7.5×10^{-16} M of ENZA, leflunomide (LEF) and teriflunomide (TER). As shown in Fig. 8, MIP@ANI-*co*-o-PD/GCE exhibited higher IF values toward ENZA than LEF and TER. The IF values for ENZA, TER, and LEF were 4.03, 1.03, and 1.02, respectively. These results clearly demonstrated that MIP@ANI-*co*-o-PD/GCE selectively bind template based on the shape and size of the ENZA compared to other species.

3.8. Interference

Na^+, SO_4^{2-}, K^+, and Cl^- as commonly found interfering ions and ascorbic acid (AA) and dopamine (DA) as well-known interfering com-

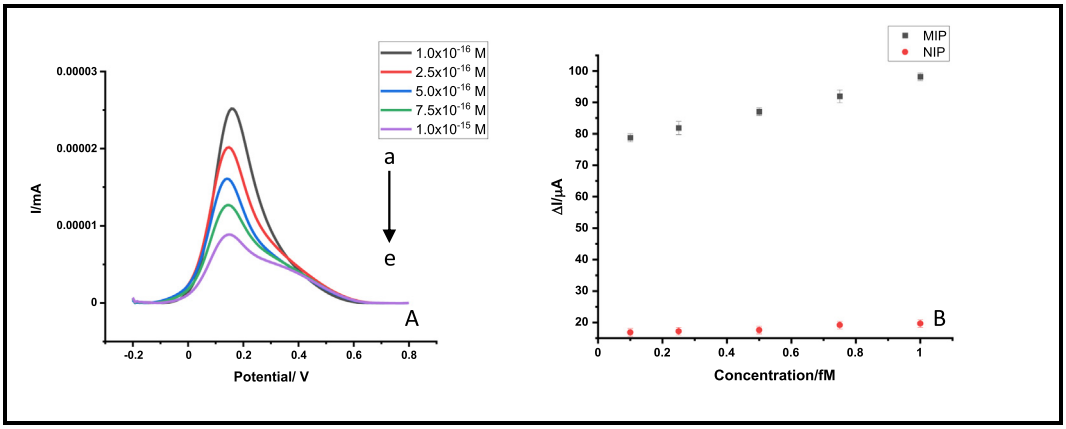

Fig. 7. **(A)** DPV of the MIP@ANI-*co*-o-PD/GCE with increasing ENZA concentration in spiked synthetic human serum sample: ENZA concentration was (a) 0.1 fM, (b) 0.25 fM, (c) 0.5 fM, (d) 0.75 fM, (e) 1 fM, respectively. **(B)** The calibration curve of ENZA using MIP@ANI-*co*-o-PD/GCE and NIP@ANI-*co*-o-PD/GCE. The measurement was performed in 5 mM $[Fe(CN)_6]^{3-/4-}$ solution/0.1 M KCl. Scan rate: 100 mV s^{-1}.

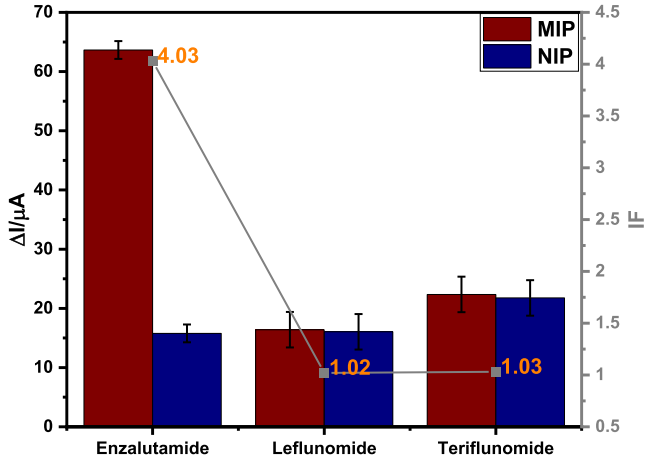

Fig. 8. The selectivity of 7.5 × 10^{-16} M ENZA compared to 7.5 × 10^{-16} M leflunomide and 7.5 × 10^{-16} M teriflunomide corresponding to MIP@ANI-*co*-o-PD/GCE and NIP@ANI-*co*-o-PD/GCE.

pounds were studied to evaluate interference-effect. Each compound was mixed with ENZA at a ratio of 1:10. RSD% values and relative errors were summarized in Table 5. Relative error values were found between 100.93% and 108.93%. These results demonstrated the good anti-interference performance of the MIP@ANI-*co*-o-PD/GCE.

3.9. Repeatability, reproducibility, and stability studies

The overall performance of a sensor is associated with good results of repeatability, reproducibility, and stability. These parameters of MIP@ANI-*co*-o-PD/GCE are summarized in Table 3. The DPV technique was utilized for investigating the repeatability and reproducibility of the sensor. The MIP@ANI-*co*-o-PD/GCE exhibited good repeatability for three successive measurements with a standard deviation (RSD) of 0.808% and 1.212% for standard and serum samples, respectively. Furthermore, reproducibility was evaluated on three different days preparing a new sensor each day. The RSD% values for each measurement at three different days using the daily prepared sensors were calculated as 1.603% 2.016% for standard and serum samples, respectively, which indicates good reproducibility. Finally, the proposed sensor has stability and reusability for 24 h and it can be used to determine all the selected concentrations in the linear range for at least six successive measurements for each concentration. These results showed that MIP@ANI-*co*-o-PD/GCE has excellent sensitivity and reusability towards ENZA.

4. Conclusion

For the first time, a voltammetric selective and sensitive sensor based on MIP@ANI-*co*-o-PD/GCE was firstly computationally designed for the precise and accurate measurement of ENZA. Furthermore, for the electrochemical detection of ENZA in serum sample and pharmaceutical dosage form, taking advantage of the selectivity of MIP and the sensitivity of the electrochemical sensor, good recovery results were obtained. The characterization of the sensor's surface morphology was performed with SEM and Raman spectroscopy methods.

This new sensor demonstrates a highly effective alternative for ENZA analysis without extensive steps such as derivatization or sample preparation. In addition, the obtained sensor is a promising alternative technique due to its low cost, easy preparation, high selectivity, and sensitivity. MIP@ANI-*co*-o-PD/GCE sensor was checked with the indirect method, $[Fe(CN)_6]^{3-/4-}$ redox marker, to monitor each step of production using DPV and CV techniques. The proposed method was achieved in a linear working concentration range of 0.1 fM-1.0 fM with a detection limit of 0.0194 fM under optimal conditions for ENZA. Moreover, this method has been satisfactorily applied in serum sample and tablets.

Table 5
Effect of interferents on the determination of ENZA.

Interferents	I = Im/Io	RSD (%)
DOP	108.93	1.32
AA	107.87	0.68
Na^+	103.52	2.10
SO_4^{2-}	103.52	2.10
K^+	100.93	1.22
Cl^-	100.93	1.22

CRediT authorship contribution statement

S. Irem Kaya: Investigation, Conceptualization, Writing – original draft. **Ahmet Cetinkaya:** Investigation, Conceptualization, Writing – original draft. **Goksu Ozcelikay:** Investigation, Conceptualization, Writing – original draft. **M. Emin Çorman:** Supervision, Conceptualization, Writing – review & editing. **Mustafa Karakaya:** Supervision, Conceptualization, Writing – review & editing. **Esen Bellur Atici:** Supervision, Conceptualization, Writing – review & editing. **Sibel A. Ozkan:** Supervision, Conceptualization, Writing – review & editing.

Declaration of Competing Interest

The authors declare that they have no known competing financial interests or personal relationships that could have appeared to influence the work reported in this paper.

Acknowledgments

Ahmet Cetinkaya thanks the financial supports from Council of Higher Education 100/2000 (YOK) under the special 100/2000 and the Scientific and Technological Research Council of Turkey (TUBITAK) under the BIDEB/2211-A PhD Scholarship Programmes. Mehmet Emin Corman thanks the Scientific and Technological Research Council of Turkey (TÜBITAK) under the BIDEB/2218- National Postdoctoral Research Fellowship Program for Turkish Citizens.

References

[1] CHMP, Assessment report for Xtandi (enzalutamide) Capsules, soft, Eur. Med. Agency. 44 (2013) 1–86.
[2] J. Semenas, N. Dizeyi, J.L. Persson, Enzalutamide as a second generation antiandrogen for treatment of advanced prostate cancer, Drug Des. Devel. Ther. 7 (2013) 875–881, https://doi.org/10.2147/DDDT.S45703.
[3] G. Butcher, H. Howard, N. Sathianathen, J.W.F. Catto, D.G. Murphy, Enzalutamide with Standard First-line Therapy in Metastatic Prostate Cancer, Eur. Urol. 76 (2019) 872–873, https://doi.org/10.1016/j.eururo.2019.07.018.
[4] Z.G. Khan, S.S. Patil, P.K. Deshmukh, P.O. Patil, Validated RP-HPLC method for determination of enzalutamide in bulk drug and pharmaceutical dosage form, Indian Drugs. 53 (11) (2016) 46–50.
[5] M. Deguigne, M. Brunet, C. Abbara, A. Turcant, G. Le Roux, B. Lelièvre, Enzalutamide and analytical interferences in digoxin assays, Clin. Toxicol. 56 (11) (2018) 1150–1154, https://doi.org/10.1080/15563650.2018.1469758.
[6] B.A. Reddy, P. Radhakrishnanand, M.I. Alam3, P.R. Kiran, A Validated Stability Indicating RP-HPLC Method Development for Anticancer Drug Enzalutamide in Bulk and Pharmaceuticals, Int. J. Pharm. Sci. Drug Res. 11 (2019) 85–90. 10.25004/ijpsdr.2019.110303.
[7] X. Ma, W. Zhou, Q. Zou, P. Ouyang, Structural elucidation of the impurities in Enzalutamide bulk drug and the development, validation of corresponding HPLC method, J. Pharm. Biomed. Anal. 131 (2016) 436–443, https://doi.org/10.1016/j.jpba.2016.08.036.
[8] A. Puszkiel, A. Plé, O. Huillard, G. Noé, C. Thibault, S. Oudard, F. Goldwasser, M. Vidal, J. Alexandre, B. Blanchet, A simple HPLC-UV method for quantification of enzalutamide and its active metabolite N-desmethyl enzalutamide in patients with metastatic castration-resistant prostate cancer, J. Chromatogr. B Anal. Technol. Biomed. Life Sci. 1058 (2017) 102–107, https://doi.org/10.1016/j.jchromb.2017.04.014.

[9] A. Zakkula, V. Kiran, U. Todmal, S. Sulochana, R. Mullangi, RP-HPLC-UV method for simultaneous quantification of second generation non-steroidal antiandrogens along with their active metabolites in mica plasma: application to a pharmacokinetic study, Drug Metab. Pharmacokinet. 69 (2019) 537–544.
[10] M.-L. Joulia, E. Carton, A. Jouinot, M. Allard, O. Huillard, N. Khoudour, M. Peyromaure, M. Zerbib, A.T. Schoemann, M. Vidal, F. Goldwasser, J. Alexandre, B. Blanchet, Pharmacokinetic/Pharmacodynamic Relationship of Enzalutamide and Its Active Metabolite N-Desmethyl Enzalutamide in Metastatic Castration-Resistant Prostate Cancer Patients, Clin. Genitourin. Cancer. 18 (2) (2020) 155–160, https://doi.org/10.1016/j.clgc.2019.05.020.
[11] L.N.R. Katakam, T. Dongala, S.K. Ettaboina, Quality by design with design of experiments approach for development of a stability-indicating LC method for enzalutamide and its impurities in soft gel dosage formulation, Biomed. Chromatogr. 35 (5) (2021), https://doi.org/10.1002/bmc.v35.510.1002/bmc.5062.
[12] D. Bennett, J.A. Gibbons, R. Mol, Y. Ohtsu, C. Williard, Validation of a method for quantifying enzalutamide and its major metabolites in human plasma by LC-MS/MS, Bioanalysis. 6 (6) (2014) 737–744, https://doi.org/10.4155/bio.13.325.
[13] A. Zhou, L. Ruan, G. Duan, J. Li, Quantitative Study of Impurities in Enzalutamide and Identification, Isolation, Characterization of Its Four Degradation Products Using HPLC, Semi-preparative LC, LC/ESI–MS and NMR Analyses, Chromatographia. 81 (11) (2018) 1519–1531, https://doi.org/10.1007/s10337-018-3611-4.
[14] S.A. Ozkan, J.-M. Kauffmann, P. Zuman, Electroanalysis in Biomedical and Pharmaceutical Sciences, Springer, Berlin, Heidelberg (2015), https://doi.org/10.1007/978-3-662-47138-8_8.
[15] S.A. Ozkan, Electroanalytical Methods in Pharmaceutical Analysis and Their Validation, HNB Pub, First edit, 2012.
[16] G. Ozcelikay, S. Kurbanoglu, B. Bozal-Palabiyik, B. Uslu, S.A. Ozkan, MWCNT/CdSe quantum dot modified glassy carbon electrode for the determination of clopidogrel bisulfate in tablet dosage form and serum samples, J. Electroanal. Chem. 827 (2018) 51–57, https://doi.org/10.1016/j.jelechem.2018.09.005.
[17] E. Turiel, A. Martín-Esteban, Molecularly imprinted polymers for sample preparation: A review, Anal. Chim. Acta. 668 (2) (2010) 87–99, https://doi.org/10.1016/j.aca.2010.04.019.
[18] B. Mattiasson, Biosensors and Molecular Imprinting (2018), https://doi.org/10.3390/books978-3-03842-563-2.
[19] Y. Yang, W. Yan, C. Guo, J. Zhang, L. Yu, G. Zhang, X. Wang, G. Fang, D. Sun, Magnetic molecularly imprinted electrochemical sensors: A review, Anal. Chim. Acta. 1106 (2020) 1–21, https://doi.org/10.1016/j.aca.2020.01.044.
[20] A. Cetinkaya, S.I. Kaya, G. Ozcelikay, E.B. Atici, S.A. Ozkan, A molecularly imprinted electrochemical sensor based on highly selective and an ultra-trace assay of anti-cancer drug axitinib in its dosage form and biological samples, Talanta. 233 (2021), https://doi.org/10.1016/j.talanta.2021.122569 122569.
[21] M.E. Çorman, A. Cetinkaya, G. Ozcelikay, E. Özgür, E.B. Atici, L. Uzun, S.A. Ozkan, A porous molecularly imprinted nanofilm for selective and sensitive sensing of an anticancer drug ruxolitinib, Anal. Chim. Acta. 1187 (2021), https://doi.org/10.1016/j.aca.2021.339143.
[22] A. Yarman, F.W. Scheller, How reliable is the electrochemical readout of MIP sensors?, Sensors (Switzerland) 20 (2020), https://doi.org/10.3390/s20092677.
[23] G. Ozcelikay, N. Karadas-Bakirhan, T. Taskin-Tok, S.A. Ozkan, A selective and molecular imaging approach for anticancer drug: Pemetrexed by nanoparticle accelerated molecularly imprinting polymer, Electrochim. Acta. 354 (2020), https://doi.org/10.1016/j.electacta.2020.136665 136665.
[24] L. Uzun, A.P.F. Turner, Molecularly-imprinted polymer sensors: Realising their potential, Biosens. Bioelectron. 76 (2016) 131–144, https://doi.org/10.1016/j.bios.2015.07.013.
[25] H.M. Mousa, J.R. Aggas, A. Guiseppi-Elie, Electropolymerization of aniline and (N-phenyl-o-phenylenediamine) for glucose biosensor application, Mater. Lett. 238 (2019) 267–270, https://doi.org/10.1016/j.matlet.2018.12.012.
[26] P. Čársky, I. Hubač, Restricted Hartree-Fock and unrestricted Hartree-Fock as reference states in many-body perturbation theory: a critical comparison of the two approaches, Theor. Chim. Acta. 80 (4-5) (1991) 407–425, https://doi.org/10.1007/BF01117420.
[27] C.C.J. Roothaan, New developments in molecular orbital theory, Rev. Mod. Phys. 23 (2) (1951) 69–89, https://doi.org/10.1103/RevModPhys.23.69.
[28] G.A. Petersson, A. Bennett, T.G. Tensfeldt, M.A. Al-Laham, W.A. Shirley, J. Mantzaris, A complete basis set model chemistry. I. The total energies of closed-shell atoms and hydrides of the first-row elements, J. Chem. Phys. 89 (4) (1988) 2193–2218, https://doi.org/10.1063/1.455064.
[29] M. Karakaya, Y. Sert, M. Kürekçi, B. Eskiyurt, Ç. Çirak, Theoretical and experimental investigations on vibrational and structural properties of tolazamide, J. Mol. Struct. 1095 (2015) 87–95, https://doi.org/10.1016/j.molstruc.2015.04.028.
[30] R. Dennington, T. Keith, J. Millam, GaussView, (2009).
[31] M.J. Frisch, G.W. Trucks, H.B. Schlegel, G.E. Scuseria, M.A. Robb, J.R. Cheeseman, G. Scalmani, V. Barone, B. Mennucci, G.A. Petersson, H. Nakatsuji, M. Caricato, X. Li, H.P. Hratchian, A.F. Izmaylov, J. Bloino, G. Zheng, J.L. Sonnenberg, M. Hada, M. Ehara, K. Toyota, R. Fukuda, J. Hasegawa, M. Ishida, T. Nakajima, Y. Honda, O. Kitao, H. Nakai, T. Vreven, J.A.M. Jr, J.E. Peralta, M.B.F. Ogliaro, J.J. Heyd, E. Brothers, K.N. Kudin, V.N. Staroverov, T. Keith, R. Kobayashi, J. Normand, K. Raghavachari, A. Rendell, J.C. Burant, S.S. Iyengar, J. Tomasi, M. Cossi, N. Rega, J. M. Millam, M. Klene, J.E. Knox, J.B. Cross, V. Bakken, C. Adamo, J. Jaramillo, R. Gomperts, R.E. Stratmann, O. Yazyev, A.J. Austin, R. Cammi, C. Pomelli, J.W. Ochterski, R.L. Martin, K. Morokuma, V.G. Zakrzewski, G.A. Voth, P. Salvador, J.J. Dannenberg, S. Dapprich, A.D. Daniels, O. Farkas, J.B. Foresman, J.V. Ortiz, J. Cioslowski, D.J. Fox, Fox Gaussian 09, Revision D.01 (2013).
[32] M. Karakaya, F. Ucun, Spectral analysis of acetylcholine halides by density functional theory calculations, J. Struct. Chem. 54 (2) (2013) 321–331, https://doi.org/10.1134/S0022476613020078.